1   **A discovery of nanoscale sulfide droplets in MORB glasses:**

2   **Implications for the immiscibility of sulfide melt and silicate**

3   **melt**

4   Lei Zuo[a], Peng Zhang[a], Rui Liu[a*], Dongping Tao[a], Xiang Liu[b], Genwen Chen[c], Kun
5   Wang[d], Gang Tao[e]

6   [a]School of Resources and Environmental Engineering, Shandong University of

7   Technology, Zibo 255000, China

8   [b]School of Economics and Management, Guangxi University of Science and

9   Technology, Liuzhou 545026, China

10   [c]Key Laboratory of Mineralogy and Metallogeny, Guangzhou Institute of Geochemistry,

11   Chinese Academy of Sciences, Guangzhou 510640, China

12   [d]Resources and Geosciences, China University of Mining and Technology, Xuzhou

13   221116, China

14   [e]School of Environment and Resource, Southwest University of Science and

15   Technology, Mianyang 621010 China

18   Corresponding authors:

19   Rui Liu, E-mail: liurui@sdut.edu.cn;

20

21

Abstract

Sulfur forms an immiscible liquid upon saturation in magma, and sulfide droplets were commonly found in fresh mid-ocean ridge basalt (MORB) magmas. In this paper, scanning electron microscopy (SEM) determined that MORB samples were primarily fine-grained and weakly phyric, with hypocrystalline to vitreous textures. A focused ion beam cut from the MORB glasses examined by transmission electron microscopy (TEM) revealed a range of nanoscale sulfide droplets (10–15 nm), featuring rounded shapes and smooth edges. Texturally, the droplets were crystalline and homogeneous in composition. Elemental S, Na, Fe, Cu, and Ni were evenly distributed within the droplets, while the content of element Si, Al and O are less in the droplets. Previous reports have elucidated the immiscibility between sulfide and silicate melts, and the structure of the silicate melt also affects the size distribution of sulfide droplets. This is the first report on nanoscale sulfide droplets within MORB glasses, and those results indicated that nanoscale sulfide droplets were the initial phase of sulfide saturation; such insight may prove useful in understanding how siderophile and chalcophile elements behaved during sulfide crystallization. In addition, this study determined the immiscibility of sulfides and silicate melts occurred in the early nanometer stage, the immiscibility of sulfides in magmatic Ni-Cu sulfide deposits was the key to the formation of magmatic Ni-Cu sulfide deposits. Therefore, all immiscibility phenomena may occur in the nanometer stage during magma evolution.

Keywords: MORB; sulfide melt; silicate melt; TEM; SEM

1. Introduction

There are two basic differentiation modes in magma evolution: segregation crystallization and immiscibility, with liquid immiscibility the more important for magma evolution (Charlier and Grove, 2012; Kamenetsky et al., 2013; Thompson et al., 2007; Veksler et al., 2008; Magloughlin, 2005). Immiscibility refers to the process by which homogeneous magma decomposes into two melts of very different compositions due to changes in temperature, pressure, composition, etc. Immiscibility has been described in a broad compositional range of natural magmas such as basalt (Skinner and Peck, 1969; De, 1974), fourchite (Philpotts, 1972), lunar rocks (Roedder and Weiblen, 1970), and various volcanic rocks (Philpotts, 1982). Sulfur forms an immiscible liquid upon saturation in magma (e.g., sulfide droplets) (Moore and Calk, 1971; Moore and Schilling, 1973; Patten et al., 2012; Yang et al., 2014). Yeats and Mathez (1976) discovered spherical iron sulfide globules in the walls of vesicles in glassy selvages of tholeiitic basalt. Czamanske and Moore (1977) discovered spherical globules in phenocrysts and glass of submarine basalt from the Mid-Atlantic Ridge.

The sulfur in MORB magma is saturated before magma eruption, and may also be saturated in the source region (Yeats and Mathez, 1976; Czamanske and Moore, 1977). Sulfide droplets were commonly reported in fresh MORB glasses (Maclean, 1969; Holzheid, 2010). Therefore, the well-preserved sulfide droplets in MORB glass provide an opportunity to study the sulfide melt-silicate melt equilibrium. (Yeats and Mathez, 1976; Czamanske and Moore, 1977; Patten et al., 2013), and these investigations indicated the sulfide droplets were commonly micro-sized and displayed zoned and fine-grained textures(Czamanske and Moore, 1977; Patten et al., 2012, 2013; Yang et al., 2014). Furthermore, during mantle melting and differentiation of basalt melt, the sulfide droplet sizes influence the physical behavior of the separate sulfide phases, and the different of sulfide droplets also plays an important role in partitioning the siderophile and cupolophile elements (Bézos et al., 2005; Czamanske and Moore, 1977; Hamlyn et al., 1985; Peach et al., 1990; Rehkämper et al., 1999; Yeats and Mathez, 1976). However, few reports have covered the formation of these sulfide droplets and subsequent scavenge of siderophile and chalcophile elements. A deeper understanding of the initial solidification of sulfide-oxide liquids remains a worthwhile endeavor.

As currently reviewed, most geological processes relate to nanoscale phenomena (Hochella et

73 al., 2008; Reich et al., 2011). For example, Hough et al. (2008) reported that nanoparticulate Au

74 develops above Au quartz veins during weathering. Gartman et al. (2014) documented that pyrite

75 nanoparticles comprise a considerable portion of black smoker emissions from hydrothermal vents,

76 and those nanoparticles may be vital sources of iron to the world's ocean (Gartman et al., 2014).

77 Deditius et al. (2018) discovered diverse mineral nanoparticles in magnetite, providing a cautionary

78 note on the interpretation of micron-scale chemical data of magnetite (Deditius et al., 2018).

79 Hawkings et al. (2020) reported that Greenland Ice Sheet meltwaters may provide biolabile

80 particulate Fe that fuels the large summer phytoplankton bloom in the Labrador Sea (Hawkings et

81 al., 2018). This indicated some nano-scale ore-processes play important roles in large-scale systems

82 (Hochella, 2002; Reich et al., 2006; Hochella et al., 2008; Hough et al., 2008).

83   Here, the material extracted in-situ from the surface of polished MORB glass samples was

84 examined by scanning electronic microscopy (SEM). A focused ion beam (FIB) with transmission

85 electron microscopy (TEM) and high-angle annular dark-field scanning transmission electron

86 microscopy (HAADF STEM) was utilized to (1) investigate micro sulfide droplets in basaltic glass

87 and (2) elucidate the premier stage of sulfide immiscibility in MORB glasses.

88 **2. Geological setting and samples**

89   The MORB samples were dredged along the axis of the SWIR during cruises DY105-17,

90 DY115-19 and DY115-20 by the R/V DaYangYiHao. The Southwest Indian Ridge (SWIR) is an

91 ultraslow-spreading ridge (Dick et al., 2003) extending from the Bouvet Triple Junction (54°50′S,

92 00°40′W) in the South Atlantic Ocean to the Rodrigues Triple Junction (25°30′S, 70°00′E) in the

93 Indian Ocean. The MORB samples in this study were chosen from the three main ridge segments

94 delimited by the Gallieni (52°20′E) and Melville (60°45′E) fracture zones (Fig. 1). As determined

95 by SEM, the MORB samples were primarily fine-grained and weakly phyric with hypocrystalline

96 to vitreous textures (Fig. 2a). Some phenocrysts were 1-10 μm and relatively rich in Si and O (Figs.

97 2b-f, 3a-d).
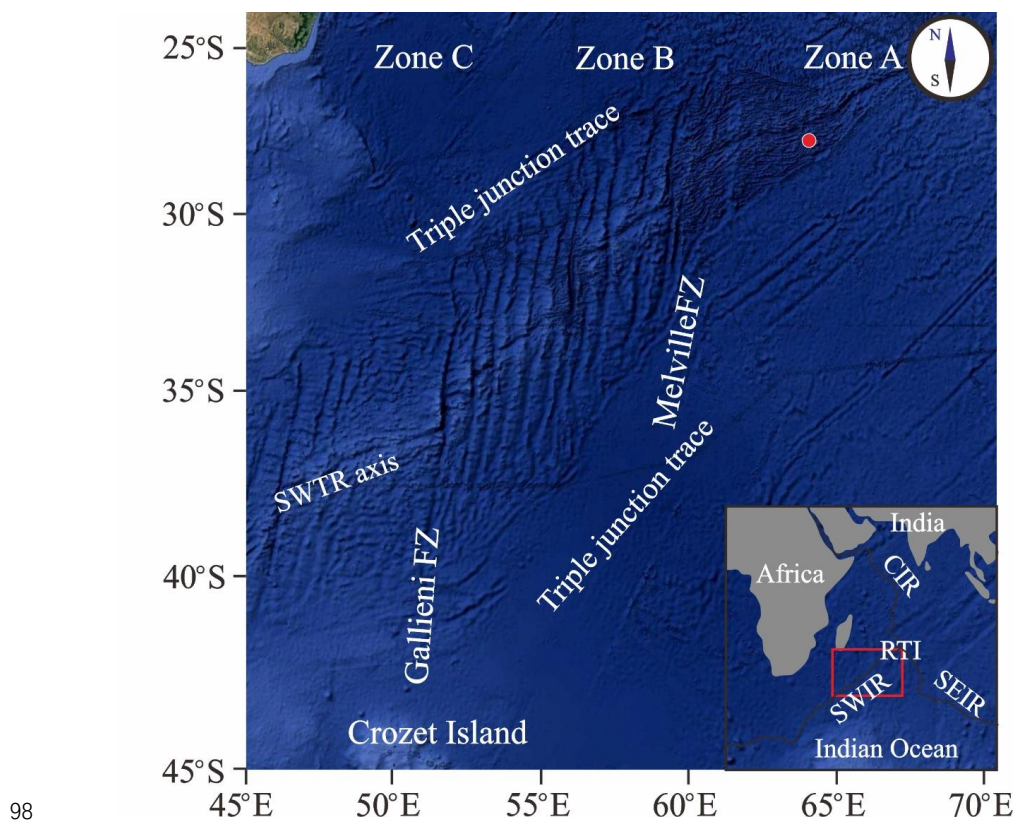
Figure 1. Regional location of the study area
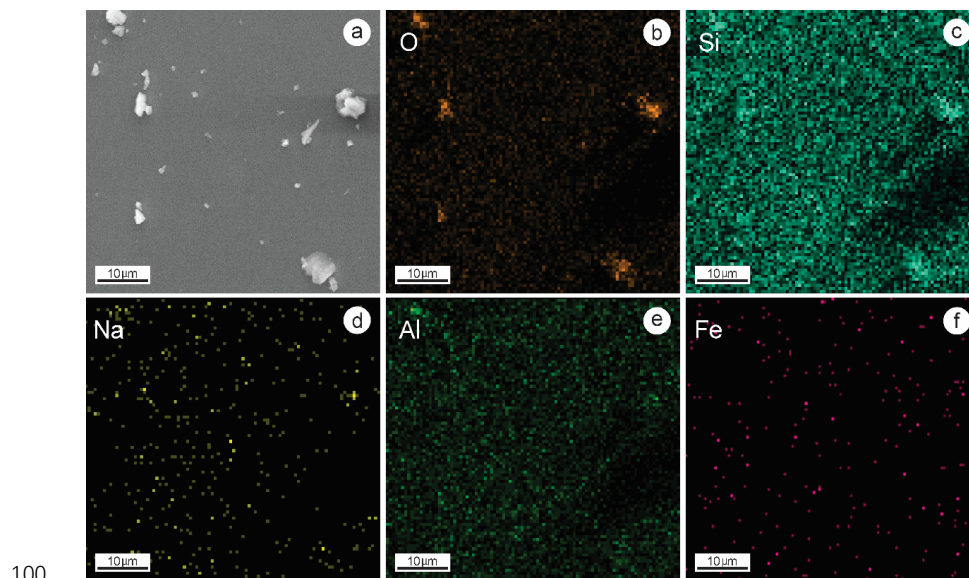
101 Figure 2. SEM image (a,) and elemental maps (b-f) of MORB samples
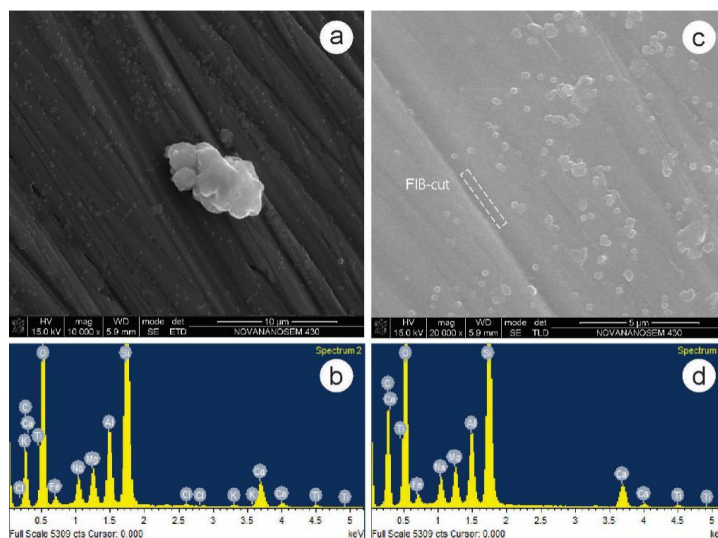
102

103 Figure 3. SEM images (a, c) of typical MORB glasses and their corresponding EDS

104 spectra (b, d).

105 **3. Materials and methods**

106   Normal microscopic analyses were conducted on polished thin petrographic sections using a

107 Zeiss-Opton light microscope with transmitted light. Rock platelets for SEM observations were

108 polished and observations conducted using a Hitachi SU8220 at 5 kV and 10 kV. Elemental

109 distribution was determined by energy dispersive X-ray spectrometry (EDS).

110   A TEM (FEI Tecnai G2 F20) equipped with an EDS detector (0.5–1 wt.% detection limit.)

111 determined the structural/chemical information about the nanoscale sulfide droplets. The maximum

112 TEM acceleration voltage was 200 kV. The TEM foil was extracted to stick on Cu grids via Pt

113 welding, and thinned to thicknesses of 50–70 nm. HAADF-STEM imaging was carried out using

114 an ultra-high resolution and probe-corrected FEI Titan Themis TEM. High-resolution transmission

115 electron microscopy (HRTEM) image processing, including Fast Fourier transform (FFT), was

116 accomplished using Gatan's Digital Micrograph software (version 3.7.4). All analyses, including

117 SEM and TEM, took place at the Sinoma Institute of Materials Research (Guangzhou) Co., Ltd.

118 **4. Results**

119   Fig. 4a shows a FIB-cut of MORB glasses that illustrated several tiny inclusions with relatively

120 high contrast. These inclusions differed in size and distributed randomly within the matrix (Fig 4b).

121 Figure 5a also shows a rounded crystalline inclusion (15 nm), based on several diffraction spots

122 recorded in the selected area electron diffraction (SAED) pattern. The lattice fringes were clearly

123 recorded in the HRTEM images except for some lattice defects (Figs. 4c and d). Another crystalline

124 round (~20 nm) inclusion, is shown in Fig. 4d. The well crystalline structure also contained lattice

125 defects as seen in (Figs. 4e and f).
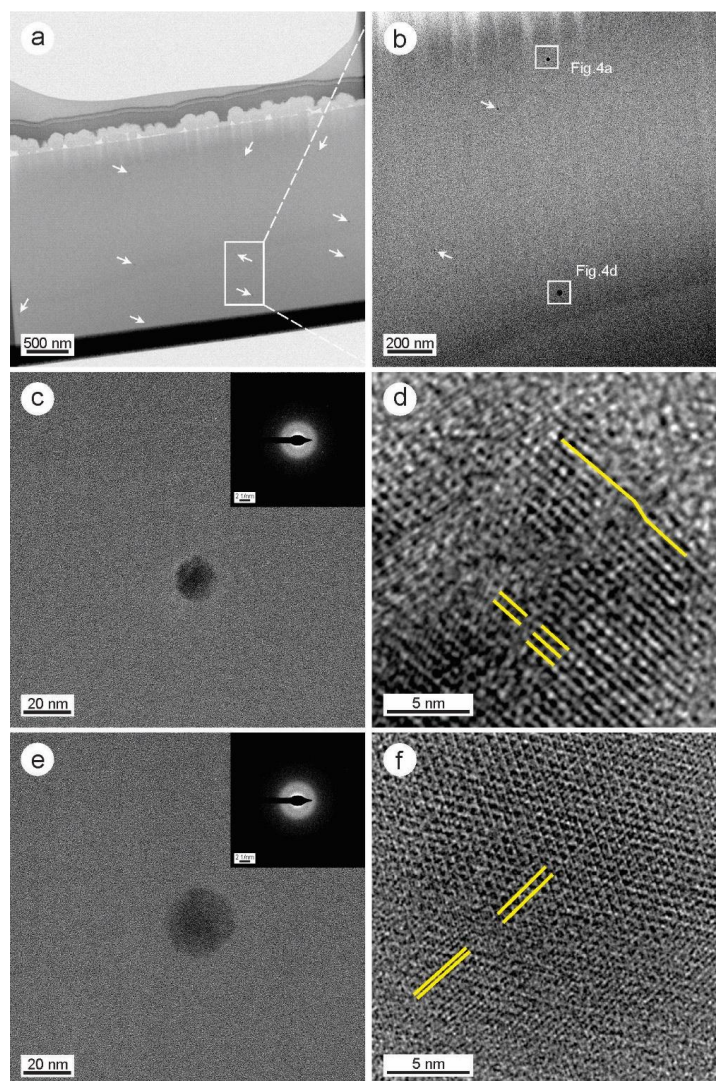
126

127 Figure 4. A focused ion beam (FIB)-cut of the MORB glasses (a, b): (a) TEM image. (b)

128 Higher magnification image obtained from the rectangle in a. (c) TEM image showing a nearly

129   rounded sulfide droplet with its SAED pattern inserted. (d) HRTEM image the droplet in b. (e)

130   TEM image showing a rounded sulfide droplet with its SAED pattern inserted. (f) HRTEM image

131   of the droplet in e.

132   Under high-angle annular dark-field scanning transmission electron microscopy (HAADF

133   STEM) imaging, the nanoscale inclusion appeared bright and consisted of metallic elements (Fig.

134   5). Compositionally, the inclusion primarily included sulfur (Table 1) that indicated these tiny

135   MORB glass inclusions were nanoscale sulfide droplets. According to elemental maps, the sulfide

136   droplet was rich in Fe, Cu, Ni and S (Fig. 6), but lacked Si, O, and Al (Fig. 7).

137   Table 1. EDS analytical data for the sulfide droplet in this study.

Element	O	Na	Mg	Al	Si	P	S	K	Ca	Ti	Mn	Fe	Ni	Cu
at. (%)	41.16	2.52	2.74	3.56	8.13	0.34	13.06	0.09	2.4	0.36	0.14	11.69	1.51	12.31
wt. (%)	20.68	1.82	2.09	3.02	7.17	0.33	13.15	0.11	3.02	0.54	0.24	20.49	2.78	24.57

138
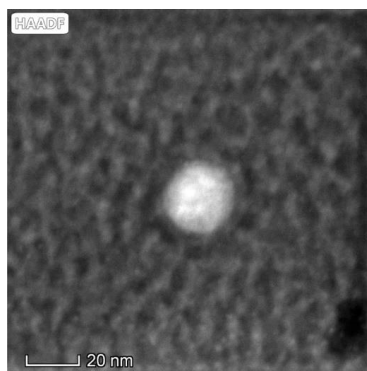
139

140   Figure 5. STEM image (a) and elemental maps (b-h) of a typical sulfide droplet within

141   MORB glasses.
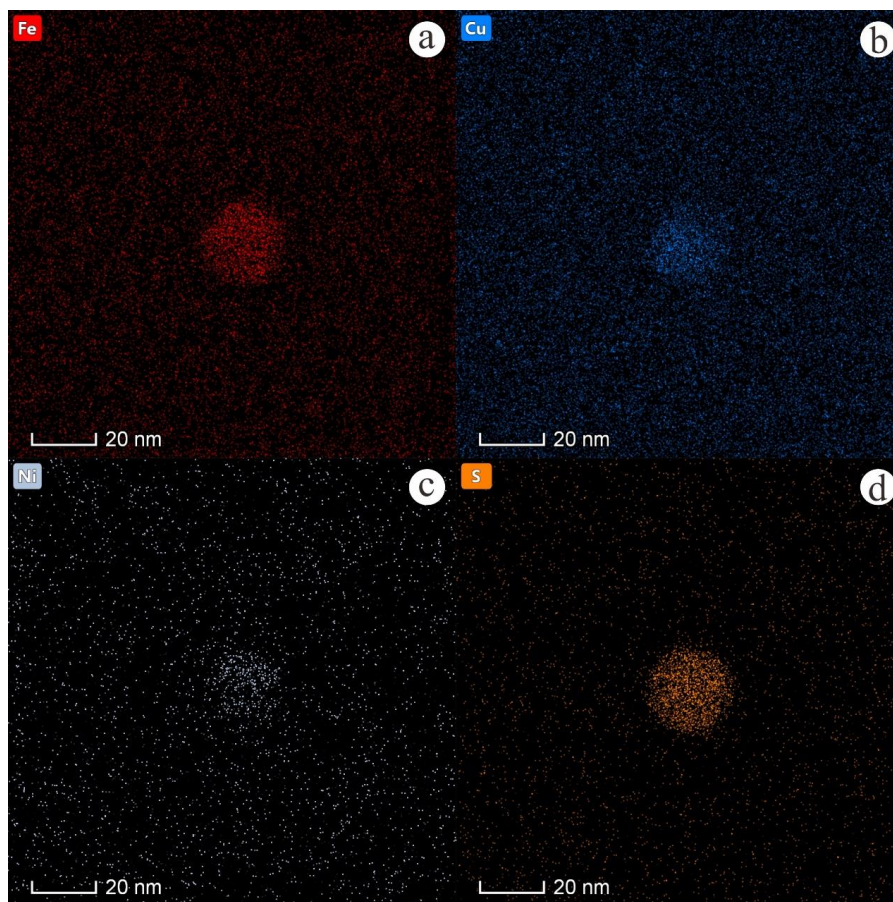
Figure 6. Elemental maps of a typical sulfide droplet within MORB glasses, the sulfide

droplets were relatively rich in Fe, Cu, Ni and S.
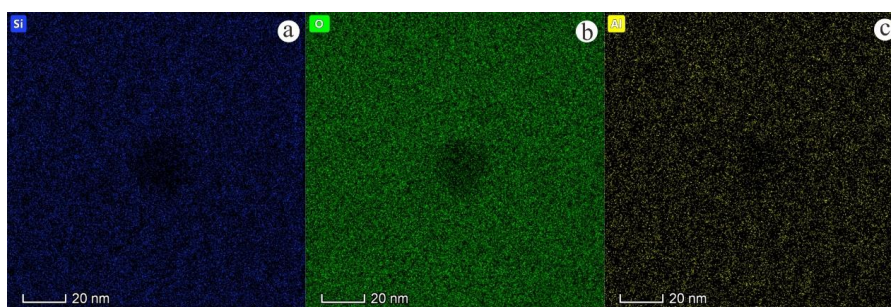
Figure 7. Elemental maps of a typical sulfide droplet within MORB glasses, the sulfide

droplets were lack in Fe, Cu, Ni and S

5. Discussion

5.1 Origin of sulfide droplets

149

150   Many studies reported the presence of sulfide globules in olivine crystals and matrix glasses

151   indicated S-saturated fractionation during magmatic evolution (Patten et al., 2012; Yang et al., 2014).

152   On one hand, well-developed sulfide globules in MORBs were thought to take shape prior to the

153   host magma quenching, like those recorded by Mathez and Yeats (1976) and Patten et al. (2012),

154   which were 5–50 μm and round in shape (Yeats and Mathez, 1976; Holzheid, 2010; Patten et al.,

155   2012). Two primary triggers lead to sulfide saturation: incipient crystallization of silicate phases

156   and falling temperature (Mavrogenes and O'Neill, 1999). On the other hand, some embayed sulfides

157   similar to those recorded by Yang et al. (2012) were thought to form from partial dissolution due to

158   decompression. In this study, nanoscale sulfide droplets in natural MORB glass are reported for the

159   first time, thus demonstrating S-saturated fractionation in another way. These recorded droplets

160   (small in size and rounded in shape) were characterized by smooth edges and crystalline features.

161   Consequently, the nanoscale sulfide droplets were more likely to form during the initial phase of

162   sulfide saturation.

5.2 The texture of sulfide droplets

163

164   Although sulfide droplets are common in fresh MORB glasses such as phenocrysts and glass,

165   microcrystalline aggregates of plagioclase and olivine, and vesicle walls (Yeats and Mathez, 1976;

166   Czamanske and Moore, 1977; Patten et al., 2012, 2013; Yang et al., 2014), the droplets (i.e., micro-

167   sized) have different textures ranging from a fine-grained intergrowth of MSS and ISS to coarser-

168   grained intergrowth of MSS and ISS with oxide and pentlandite (Yeats and Mathez, 1976;

169   Czamanske and Moore, 1977). The textural differences of these droplets might be controlled by

170   component nucleation and diffusion rates (Czamanske and Moore, 1977). For example, Patten et al.

171   (2013) reported that fine-grained and coarse-grained droplets correspond to the primitive sulfide

172   liquid and the zoned sulfide droplets correspond to the stage where MSS crystallized and co-existed

173   with a residual sulfide liquid (the quenched ISS) (Patten et al., 2013). Compared with those micro-

174   sized sulfide droplets with various textures (Patten et al., 2013; Yang et al., 2012), the nanoscale

175   sulfide droplets recorded in this paper differed significantly in terms of internal textures showing

176   homogeneous compositions without internal fractionation of MSS and ISS phases. Beyond that, the

177   sulfide droplets in this study were crystalline, and their lattices possibly formed during this stage

178 (Fig. 4c-f).

179   On the other hand, the sulfide droplet sizes varied at different stages of sulfur saturation, and

180 the droplet sizes also controlled the textural differences of the droplets. Holzheid (2010) showed the

181 polymerization degree of the silicate liquid controlled the sulfide droplet size distribution. Patten et

182 al. (2012) speculated a positive correlation between the droplet diameter increase and the degree of

183 phase segregation. Beyond that, Peach et al. (1990) reported that the size of a globule should reflect

184 its residence time in the melt and the frequency with which it contacts and consumes other globules.

185 Ostwald's ripening plays an important role in globule size change (Yang et al., 2014). The

186 experimental results show that when the composition of silicate melt becomes immiscible, two-

187 phase nanoscale droplets will soon appear. Small droplets then disappear, which enlarges the larger

188 droplets, and this process is generally accompanied by a reduction in interface free energy (Mazurin

189 and Porai-Koshits, 1984). In this study, the nanoscale sulfide droplets were small (10–15 nm) and

190 have rounded shapes and smooth edges. In summary, sulfides appeared to form very shortly before

191 eruption, followed by immediate supercooling.

5.3 Implications for sulfide droplets scavenge siderophile and chalcophile elements

193   Sulfide plays an important role in the distribution of sulfurophile elements during mantle

194 melting and basalt melt differentiation (Mathez, 1976; Peach et al., 1990; Bezos et al., 2005). When

195 the sulfide melt droplets segregated, the droplets scavenged siderophile and chalcophile elements

196 such as Ni, Cu, Pt, and Pd from the magma (Holzheid, 2010). Most micro-sized sulfide grains in

197 MORBs contained MSS , the first mineral to crystallize from a sulfide liquid, and ISS, which

198 crystallizes from the remaining liquid (Patten et al., 2013). As such the distributions of different

199 chalcophile elements regarding partition preference commonly behave differently in MSS and ISS.

200 For instance, platinum-group elements (PGE) are scavenged by immiscible sulfides during the

201 evolution of mafic magmas (Keays, 1995; Peach et al., 1990; Rehkämper et al., 1999; Song et al.,

202 2006), but the iridium-subgroup of PGE (Os, Ir, Ru, and Rh) normally behave as compatible

203 elements and partition into MSS (Patten et al., 2013; Yang et al., 2014). Co and Re have a slight

204 preference for MSS, whereas Cu, Zn, Au, Ag, Sn, Te, Cd, Bi, and Pb partition into ISS (Patten et

205 al., 2013). The sulfide droplets reported in Yang et al. (2014) contained Ni-Fe-rich MSS and Cu-

206 Fe-rich ISS phases.

207   However, the existing literature does not specify exactly when the sulfurphilic elements enter

208   the sulfide droplets. Different from micro-sized droplets, the nanoscale sulfide droplets in this study

209   compositionally contained Fe, Cu, Ni and S (Fig. 6). These elements might have been scavenged

210   during initial sulfide saturation and behaved similarly in the droplets. With the formation of sulphide

211   beads, the elements Si, O and Al are depleted at the same time. Based on the nanoscale sulfide

212   droplets reported in this paper, chalcophile elements appeared to enter the sulfide droplets and

213   distribute evenly within the sulfide globule in the early stage. As sulfide droplets in MORB provide

214   unique records of near-liquidus phase relations in basaltic systems, such insight help understand

215   how chalcophile elements behaved during sulfide crystallization. With longer residence times,

216   sulfide droplets gradually evolved and featured different textures including MSS and ISS, in which

217   different chalcophile elements had their own preferences.

5.4 Implications of sulfide droplets on magmatic evolution and formation of sulfide deposits

219   Immiscibility is an important factor in the process of magmatic evolution and mineralization.

220   During magma immiscibility, a single component melt can decompose into two kinds of melts with

221   completely different compositions. After magma immiscibility, the large-scale separation of

222   conjugated two-phase melts affects the overall evolution of magma. The earlier immiscibility begins

223   in the process of magmatic evolution, the better its influence on magmatic evolution, and the better

224   its geochemical and petrological significance (Veksler et al., 2008). Therefore, understanding the

225   nucleation, growth and separation of immiscible droplets is very important to understand the role of

226   immiscibility in magmatic evolution. As one of the immiscible phases, the immiscibility of sulfide

227   droplets and silicate melt plays an important role in magmatic evolution. The immiscibility between

228   sulfide and silicate melts has been clearly elucidated in previous studies. The basic principle of

229   magmatic sulfide deposits origins stems from the sulfur saturation of magma (Mungall and Naldrett,

230   2008). Sulfide droplets form when sulfur saturation occurs. Magmatic sulfide deposits form when

231   sulfide droplets become sufficiently concentrated enough in a certain area of the magmatic body

232   (Mungall and Naldrett, 2008). The study shows that the formation of magmatic Ni-Cu sulfide

233   deposits is related to the separation and enrichment of sulfur saturated and immiscible sulfide liquids

234   in mantle-derived basic and ultrabasic magmas (Arndt et al., 2005).

235   According to the elemental maps, the sulfide droplets were relatively rich in Fe, Cu, Ni and S

236 (Fig. 6), but lacking in Si, O, and Al (Fig. 7); this indicated the immiscibility of sulfide and silicate

237 melts occurred during the early stage. According to the results, the immiscibility of sulfide and

238 silicate melt occurs in the nanoscale stage, so it can be inferred that the immiscibility in the process

239 of magma evolution may occur in the nanoscale stage.

240 **6. Conclusions**

241   Nanoscale sulfide droplets were first identified in MORB glasses by FIB-cut and TEM analyses.

242 These droplets might form rapidly before eruption and then undergo immediate supercooling. As

243 the initial phase of sulfide saturation, nanoscale sulfide droplets simultaneously scavenged Fe, Cu,

244 Ni, and Na in the early stage rather than selectively concentrating siderophile and chalcophile

245 elements in different parts of the droplet. Furthermore, this new understanding of sulfide and silicate

246 melt immiscibility, which occurs during the early nanometer stage provides a new idea for further

247 study of the immiscibility stage during magma evolution.

248 **Declaration of Competing Interest**

249   The authors declare that they have no known competing financial interests or personal

250 relationships that could have appeared to influence the work reported in this paper.

251 **Acknowledgments**

252   This research was supported by the National Natural Science Foundation of China (Grant Nos.

253 42102076), project ZR2021QD037 supported by Shandong Provincial Natural Science Foundation,

254 and the Guangdong Basic and Applied Basic Research Foundation (2020A1515010906)

255

256   **Reference**

257   Arndt, N.T., Lesher, C.M.,Czamanske, G.K.: Mantle-derived magmas and magmatic Ni-Cu-(PGE)

258   deposits, https://doi.org/10.5382/AV100.02, 2005.

259   Bézos, A., Lorand, J. P., Humler, E., and Gros, M.: Platinum-group element systematics in Mid-

260   Oceanic Ridge basaltic glasses from the Pacific, Atlantic, and Indian Oceans, Geochim. Cosmochim.

261   Acta, 69, 2613–2627, https://doi.org/10.1016/j.gca.2004.10.023, 2005.

262   Charlier, B. and Grove, T. L.: Experiments on liquid immiscibility along tholeiitic liquid lines of

263   descent, Contrib. to Mineral. Petrol., 164, 27–44, https://doi.org/10.1007/s00410-012-0723-y, 2012.

264   Czamanske, G. K. and Moore, J. G.: Composition and phase chemistry of sulfide globules in basalt

265   from the Mid-Atlantic Ridge rift valley near 37°N lat, Bull. Geol. Soc. Am., 88, 587–599,

266   https://doi.org/10.1130/0016-7606(1977)88<587:CAPCOS>2.0.CO;2, 1977.

267   De, A.: Silicate liquid immiscibility in the Deccan Traps and its petrogenetic significance, Bull. Geol.

268   Soc. Am., 85, 471–474, https://doi.org/10.1130/0016-7606(1974)85<471:SLIITD>2.0.CO;2, 1974.

269   Deditius, A. P., Reich, M., Simon, A. C., Suvorova, A., Knipping, J., Roberts, M. P., Rubanov, S.,

270   Dodd, A., and Saunders, M.: Nanogeochemistry of hydrothermal magnetite, Contrib. to Mineral.

271   Petrol., 173, 1–20, https://doi.org/10.1007/s00410-018-1474-1, 2018.

272   Gartman, A., Findlay, A. J., and Luther, G. W.: Nanoparticulate pyrite and other nanoparticles are a

273   widespread component of hydrothermal vent black smoker emissions, Chem. Geol., 366, 32–41,

274   https://doi.org/10.1016/j.chemgeo.2013.12.013, 2014.

275   Hamlyn, P. R., Keays, R. R., Cameron, W. E., Crawford, A. J., and Waldron, H. M.: Precious metals in

276   magnesian low-Ti lavas: Implications for metallogenesis and sulfur saturation in primary magmas,

277   Geochim. Cosmochim. Acta, 49, 1797–1811, https://doi.org/10.1016/0016-7037(85)90150-4, 1985.

278   Hawkings, J. R., Benning, L. G., Raiswell, R., Kaulich, B., Araki, T., Abyaneh, M., Stockdale, A.,

279   Koch-Müller, M., Wadham, J. L., and Tranter, M.: Biolabile ferrous iron bearing nanoparticles in

280   glacial sediments, Earth Planet. Sci. Lett., 493, 92–101, https://doi.org/10.1016/j.epsl.2018.04.022,

281   2018.

282   Hochella, M. F.: Nanoscience and technology: The next revolution in the Earth sciences, Earth Planet.

283   Sci. Lett., 203, 593–605, https://doi.org/10.1016/S0012-821X(02)00818-X, 2002.

284   Hochella, M. F., Lower, S. K., Maurice, P. A., Penn, R. L., Sahai, N., Sparks, D. L., and Twining, B.

285   S.: Nanominerals, mineral nanoparticles, and earth systems, Science (80-.)., 319, 1631–1635,

286   https://doi.org/10.1126/science.1141134, 2008.

287   Holzheid, A.: Separation of sulfide melt droplets in sulfur saturated silicate liquids, Chem. Geol., 274,

288   127–135, https://doi.org/10.1016/j.chemgeo.2010.03.005, 2010.

289   Hough, R. M., Noble, R. R. P., Hitchen, G. J., Hart, R., Reddy, S. M., Saunders, M., Clode, P.,

290   Vaughan, D., Lowe, J., Gray, D. J., Anand, R. R., Butt, C. R. M., and Verrall, M.: Naturally occurring

291   gold nanoparticles and nanoplates, Geology, 36, 571–574, https://doi.org/10.1130/G24749A.1, 2008.

292   Kamenetsky, V. S., Charlier, B., Zhitova, L., Sharygin, V., Davidson, P., and Feig, S.: Magma

293   chamber-scale liquid immiscibility in the siberian traps represented by melt pools in native iron,

294   Geology, 41, 1091–1094, https://doi.org/10.1130/G34638.1, 2013.

295   Keays, R.: The role of komatiitic and picritic magmatism and S-saturation in the formation of ore

296   deposits, Lithos, 34, 1–18, https://doi.org/10.1016/0024-4937(94)00029-2, 1995.

297   Mathez, E. A.: Sulfur Solubility and Magmatic Sulfides in Submarine Basalt Glass., J Geophys Res,

298   81, 4269–4276, https://doi.org/10.1029/JB081i023p04269, 1976.

299   Mavrogenes, J. A. and O'Neill, H. S. C.: The relative effects of pressure, temperature and oxygen

300   fugacity on the solubility of sulfide in mafic magmas, Geochim. Cosmochim. Acta, 63, 1173–1180,

301   https://doi.org/10.1016/S0016-7037(98)00289-0, 1999.

302   Mazurin, O.V. and Porai-Koshits, E.A.: Phase separation in glass, 1984.

303   Moore, J. G. and Schilling, J. G.: Vesicles, water, and sulfur in Reykjanes Ridge basalts, Contrib. to

304   Mineral. Petrol., 41, 105–118, https://doi.org/10.1007/BF00375036, 1973.

305   Patten, C., Barnes, S. J., and Mathez, E. A.: Textural variations in morb sulfide droplets due to

306   differences in crystallization history, Can. Mineral., 50, 675–692,

307   https://doi.org/10.3749/canmin.50.3.675, 2012.

308   Patten, C., Barnes, S. J., Mathez, E. A., and Jenner, F. E.: Partition coefficients of chalcophile elements

309   between sulfide and silicate melts and the early crystallization history of sulfide liquid: LA-ICP-MS

310   analysis of MORB sulfide droplets, Chem. Geol., 358, 170–188,

311   https://doi.org/10.1016/j.chemgeo.2013.08.040, 2013.

312   Peach, C.L., Mathez, E. A., and Keays, R.R.: Sulfide melt-silicate melt distribution coefficients for

313   noble metals and other chalcophile elements as deduced from MORB: Implications for partial melting,

314   Geochimica et Cosmochimica Acta, 54, 3379-3389, https://doi.org/10.1016/0016-7037(90)90292-S,

315   1990.

316   Philpotts, A. R.: Density, surface tension and viscosity of the immiscible phase in a basic, alkaline

317   magma, Lithos, 5, 1–18, https://doi.org/10.1016/0024-4937(72)90076-X, 1972.

318   Philpotts, A. R.: Compositions of immiscible liquids in volcanic rocks, Contrib. to Mineral. Petrol., 80,

319   201–218, https://doi.org/10.1007/BF00371350, 1982.

320   Rehkämper, M., Halliday, A. N., Fitton, J. G., Lee, D. C., Wieneke, M., and Arndt, N. T.: Ir, Ru, Pt,

321   and Pd in basalts and komatiites: New constraints for the geochemical behavior of the platinum-group

322   elements in the mantle, Geochim. Cosmochim. Acta, 63, 3915–3934, https://doi.org/10.1016/S0016-

323   7037(99)00219-7, 1999.

324   Reich, M., Utsunomiya, S., Kesler, S. E., Wang, L., Ewing, R. C., and Becker, U.: Thermal behavior of

325   metal nanoparticles in geologic materials, Geology, 34, 1033–1036,

326   https://doi.org/10.1130/G22829A.1, 2006.

327   Reich, M., Hough, R. M., Deditius, A., Utsunomiya, S., Ciobanu, C. L., and Cook, N. J.:

328   Nanogeoscience in ore systems research: Principles, methods, and applications. Introduction and

329   preface to the special issue, Ore Geol. Rev., 42, 1–5, https://doi.org/10.1016/j.oregeorev.2011.06.007,

330   2011.

331   Song, X. Y., Zhou, M. F., Keays, R. R., Cao, Z. M., Sun, M., and Qi, L.: Geochemistry of the

332   Emeishan flood basalts at Yangliuping, Sichuan, SW China: Implications for sulfide segregation,

333   Contrib. to Mineral. Petrol., 152, 53–74, https://doi.org/10.1007/s00410-006-0094-3, 2006.

334   Thompson, A. B., Aerts, M., and Hack, A. C.: Liquid immiscibility in silicate melts and related

335   systems, Rev. Mineral. Geochemistry, 65, 99–127, https://doi.org/10.2138/rmg.2007.65.4, 2007.

336   Veksler, I. V., Dorfman, A. M., Borisov, A. A., Wirth, R., and Dingwell, D. B.: Liquid immiscibility

337   and evolution of basaltic magma: Reply to S. A. Morse, A. R. McBirney and A. R. Philpotts, J. Petrol.,

338   49, 2177–2186, https://doi.org/10.1093/petrology/egn064, 2008.

339   Yang, A. Y., Zhou, M. F., Zhao, T. P., Deng, X. G., Qi, L., and Xu, J. F.: Chalcophile elemental

340   compositions of MORBs from the ultraslow-spreading Southwest Indian Ridge and controls of

341   lithospheric structure on S-saturated differentiation, Chem. Geol., 382, 1–13,

342   https://doi.org/10.1016/j.chemgeo.2014.05.019, 2014.

343   Yeats, R. S. and Mathez, E. A.: Decorated Vesicles in Deep-Sea Basalt Glass, Eastern Pacific., J

344   Geophys Res, 81, 4277–4284, https://doi.org/10.1029/JB081i023p04277, 1976.

345